JACS
JOURNAL OF THE AMERICAN CHEMICAL SOCIETY
Article
pubs.acs.org/JACS

From Yellow to Black: Dramatic Changes between Cerium(IV) and Plutonium(IV) Molybdates

Justin N. Cross,[†] Patrick M. Duncan,[†] Eric M. Villa,[†] Matthew J. Polinski,[†] Jean-Marie Babo,[†] Evgeny V. Alekseev,[‡,§] Corwin H. Booth,[∥] and Thomas E. Albrecht-Schmitt*[,⊥]

[†]Department of Chemistry and Biochemistry and Department of Civil Engineering and Geological Sciences, University of Notre Dame, 156 Fitzpatrick Hall, University of Notre Dame, Notre Dame, Indiana 46556, United States

[‡]Institute for Energy and Climate Research (IEK-6), Forschungszentrum Jülich GmbH, 52428 Jülich, Germany

[§]Institut für Kristallographie, RWTH Aachen University, 52066 Aachen, Germany

[∥]Chemical Sciences Division, Lawrence Berkeley National Laboratory, Berkeley, California 94720, United States

[⊥]Department of Chemistry and Biochemistry, Florida State University, 95 Chieftan Way, 310 DLC, Tallahassee, Florida 32306-4390, United States

Supporting Information

ABSTRACT: Hydrothermal reactions of $CeCl_3$ and $PuCl_3$ with MoO_3 and Cs_2CO_3 yield surprisingly different results. $Ce_3Mo_6O_{24}(H_2O)_4$ crystallizes as bright yellow plates (space group $C2/c$, a = 12.7337(7) Å, b = 22.1309(16) Å, c = 7.8392(4) Å, β = 96.591(4)°, V = 2194.6(2) Å^3), whereas $CsPu_3Mo_6O_{24}(H_2O)$ crystallizes as semiconducting black-red plates (space group $C2/c$, a = 12.633(5) Å, b = 21.770(8) Å, c = 7.743(7) Å, β = 96.218(2)°, V = 2117(2) Å^3). The topologies of the two compounds are similar, with channel structures built from disordered Mo(VI) square pyramids and $(RE)O_8$ square antiprisms (RE = Ce(IV), Pu(IV)). However, the Pu(IV) compound contains Cs^+ in its channels, while the channels in $Ce_3Mo_6O_{24}(H_2O)_4$ contain water molecules. Disorder and an ambiguous oxidation state of Mo lead to the formula $CsPu_3Mo_6O_{24}(H_2O)$, where one Mo site is Mo(V) and the rest are Mo(VI). X-ray absorption near-edge structure (XANES) experiments were performed to investigate the source of the black color of $CsPu_3Mo_6O_{24}(H_2O)$. These experiments revealed Pu to be tetravalent, while the strong pre-edge absorption from the distorted molybdate anions leaves the oxidation state ambiguous between Mo(V) and Mo(VI).

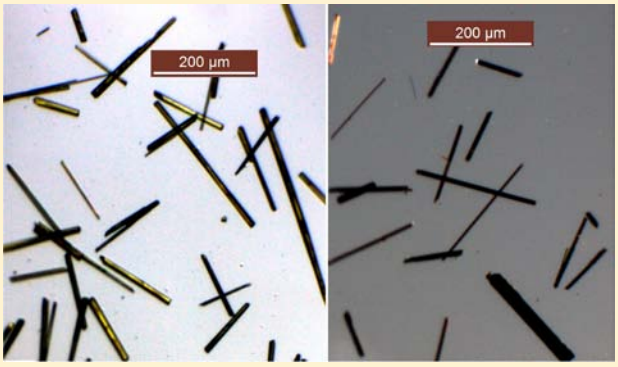

INTRODUCTION

The term surrogate has been widely applied to the use of non- or less-radioactive elements in the place of shorter-lived isotopes that are more challenging to investigate. This replacement is particularly common with plutonium, where Ce(IV) has been used to replace Pu(IV) and Nd(III) has been used to replace Pu(III). This substitution is based on nearly identical ionic radii, and the chemistry is in fact often very similar. In an effort to move away from the use of surrogates in actinide chemistry, recent studies have clearly shown the differences between lanthanide and actinide compounds when they are synthesized under similar conditions. In the trivalent state, the rare-earth borate series has displayed significant structural differences between the lanthanides and actinides, in both the local coordination of the metal center and the borate network.[1−3] Computational studies of these systems reveal that the differences in structures and local coordination environments are a direct consequence of covalency between the 6p or 6d orbitals and ligand orbitals with Pu(III), Am(III), and Cm(III), a feature that is completely absent in lanthanides. In the tetravalent state, discrepancies have been shown between Ce(IV) and Pu(IV) as well as between early An(IV) and transuranic An(IV).[4−14] Exploration of this field is filled with opportunity, as there are only a few systems that have systematically spanned the lanthanide and actinide series such as the aquo-triflates, phosphonates, and phosphites.[15−25] It is in this objective that we have chosen to explore the f-block molybdates.

Molybdenum oxoanions are well-known to be highly distorted due to second-order Jahn−Teller effects which give rise to a Mo(VI) center that can adopt several different geometries. Molybdates can be octahedral, square pyramidal, trigonal bipyramidal, and tetrahedral. The adoption of coordination geometries lacking an inversion center makes it an attractive ligand to produce noncentrosymmetric compounds.[26−33] In addition, Mo^{VI}−O bonds are highly polarizable like borate, and therefore differences in reactivity between Pu(IV) and Ce(IV) may be realized if this polarization of electron density leads to covalent

Received: December 6, 2012
Published: January 29, 2013

   dx.doi.org/10.1021/ja311910h | J. Am. Chem. Soc. 2013, 135, 2769−2775

bonding, even if the effects are minor. Furthermore, much like borate, molybdate can form polymeric networks that are likely to rearrange as a consequence of metal complexation. What differentiates molybdate from borate is that it is redox active and stabilizes Pu(IV) instead of Pu(III).

Molybdates are also important to the spent nuclear fuel cycle. Molybdenum is a fission product, and the formation of plutonium molybdates has been suggested as a means of creating insoluble products from the dissolution of breached zirconium-clad fuel rods, limiting the mobility of Pu into the environment.[34] Molybdate phases also form from the alteration of spent nuclear fuel during burn-up and have a large impact on the mobility of all actinides in a repository-type environment.[35]

The environmental importance and structural complexity of molybdate have driven a large research effort in the structural chemistry of actinyl molybdates and, to a smaller extent, the trivalent and tetravalent actinide molybdates.[36−41] Concurrently, lanthanide molybdates have also been investigated for their complex and interesting properties, such as negative thermal expansion, ferroelectricity, ferroelasticity, photoluminescence, and interesting structure types.[42−49] Of particular interest is the compound Ce_2MoO_6 of the Ln_2MoO_6 series (Ln = La−Lu). Ce_2MoO_6 is unusual with respect to the rest of the series, as it adopts a black color while the others assume their typical colors and appears to adopt a structure unique to the series. Its anomalous properties were attributed to mixed valency from either Ce or Mo.[50,51] Soderholm et al. carried out a series of investigations on Ce_2MoO_6 to determine the valence state of both Ce and Mo using X-ray absorbance measurements and to determine accurate unit cell constants using neutron diffraction. They found that within the limits of their experiment all Ce was trivalent and all the molybdenum was hexavalent, attributing the properties to oxygen vacancies.[52−54] Herein we report a new Pu(IV) molybdate of a black color, $CsPu_3Mo_6O_{24}(H_2O)$, which contrasts greatly with its congener Ce(IV) in the bright yellow $Ce_3Mo_6O_{24}(H_2O)_4$. Although both share similar reaction paths, oxidizing from RE(III) to RE(IV), and structural topologies consisting of channel structures built of disordered molybdate square pyramids, the similarities end there. We use RE in this work to describe Ce and Pu for ease of understanding and simplicity. The actinides are traditionally not considered rare earths, but contemporarily they have been described as such. The channels of $Ce_3Mo_6O_{24}(H_2O)_4$ contain water molecules, whereas the channels of $CsPu_3Mo_6O_{24}(H_2O)$ contain Cs^+ cations. Additionally, the plutonium compound is a semiconductor with a band gap of 1.20 ± 0.03 eV while the cerium compound is a wide band gap semiconductor with a gap of 2.68 ± 0.02 eV.

EXPERIMENTAL SECTION

Syntheses. $CeCl_3$ (99.9%, Alfa Aesar) and Cs_2CO_3 (99.9%, Alfa Aesar) were used as obtained. Weapons grade plutonium (94% ^{239}Pu, 6% ^{240}Pu) in the form of $PuCl_3$ was used as received from LANL. Reactions were run in PTFE-lined Parr 4749 autoclaves with a 23 mL internal volume for the lanthanides and with a 10 mL internal volume autoclave for plutonium. Deionized water was used in all reactions. *Caution! ^{239}Pu ($t_{1/2}$ = 24065 y) and ^{240}Pu ($t_{1/2}$ = 6537 y) represent serious health risks, owing to their α and γ emission. All studies with plutonium were conducted in a laboratory dedicated to studies on transuranium elements. This laboratory is located in a nuclear science facility and is equipped with HEPA filtered hoods and negative pressure gloveboxes that are ported directly into the hoods. A series of counters continually monitor radiation levels in the laboratory. The laboratory is licensed by the Nuclear Regulatory Commission. All experiments were carried out with approved safety operating procedures. All free-flowing solids are worked with in gloveboxes, and products are only examined when coated with either water or Krytox oil and water. There are significant limitations in accurately determining yields with plutonium compounds, because this requires drying, isolating, and weighing a solid, which poses certain risks, as well as manipulation difficulties given the small quantities employed in the reactions.*

$CsPu_3Mo_6O_{24}(H_2O)$. $PuCl_3$ (0.0105 g, 0.0301 mmol), MoO_3 (0.005 g 0.0343 mmol), Cs_2CO_3 (0.0071 g, 0.022 mmol), and 150 μL of H_2O were loaded into a 10 mL autoclave. The autoclave was sealed and heated to 200 °C in a box furnace in an argon-filled glovebox for 5 days. The autoclave was then cooled to room temperature at a rate of 5 °C/h. The products were rinsed with water, and thin black plates were isolated.

$Ce_3Mo_6O_{24}(H_2O)_4$. $CeCl_3$ (0.0493 g, 0.200 mmol), MoO_3 (0.0287g 0.200 mmol), Cs_2CO_3 (0.652 g, 0.200 mmol), and 2.0 mL of H_2O were loaded into a 23 mL autoclave. The autoclave was sealed and heated to 200 °C in a box furnace for 5 days. The autoclave was then cooled to room temperature at a rate of 5 °C/h. The products were rinsed with water, and yellow acicular crystals were isolated. Yellow plates were also obtained from this reaction; however, suitable crystals for SCXRD could not be found. Similar results were obtained on substituting K_2CO_3 for Cs_2CO_3. It was found that addition of 1 molar equiv of a mild oxidizing agent such as $Te(OH)_6$ increased the yield.

Crystallographic Studies. Single crystals of $CsPu_3Mo_6O_{24}(H_2O)$ and $Ce_3Mo_6O_{24}(H_2O)_4$ were mounted on cryoloops with viscous Krytox and optically aligned on a Bruker APEXII Quazar X-ray diffractometer using a digital camera. Crystallographic data for the two compounds are given in Table 1. Initial intensity measurements were performed using a IμS X-ray source (MoKα, λ = 0.71073 Å) with high-brilliance and high-performance focusing Quazar multilayer optics. Standard APEXII software was used for determination of the unit cells and data collection control. The intensities of reflections of a sphere were collected by a combination of multiple sets of exposures (frames). Each set had a different φ angle for the crystal, and each exposure covered a range of 0.5° in ω. For $Ce_3Mo_6O_{24}(H_2O)_4$ a total of 2762 images with an exposure time of 20 s were collected. For $CsPu_3Mo_6O_{24}(H_2O)$ a total of 1464 images with an exposure time of 40 s were collected. The SAINT software was used for data integration, including Lorentz and polarization corrections. Both crystals were nonmerohedrally twinned with a rotation angle of 180°.

Table 1. Crystallographic Data for $CsPu_3Mo_6O_{24}(H_2O)$ and $Ce_3Mo_6O_{24}(H_2O)_4$

	$CsPu_3Mo_6O_{24}(H_2O)$	$Ce_3Mo_6O_{24}(H_2O)_4$
formula mass (amu)	1850.55	1455.0
color, habit	black, plate	yellow, plate
space group	*C*2/*c*	*C*2/*c*
a (Å)	12.633(5)	12.7337(7)
b (Å)	21.770(8)	22.1309(16)
c (Å)	7.743(7)	7.8392(4)
α (deg)	90	90
β (deg)	96.218(2)	96.591(4)
γ (deg)	90	90
V (Å^3)	2117(2)	2194.6(2)
Z	4	4
T (K)	100	100
λ (Å)	0.71073	0.71073
max 2*θ* (deg)	27.48	27.53
ρ_{calcd} (g cm^{-3})	5.806	4.380
μ(Mo K*α*) (cm^{-1})	1444.1	951.7
$R(F)$ for $F_o^2 > 2\sigma(F_o^2)^a$	0.0417	0.0403
$R_w(F_o^2)^b$	0.0626	0.0632

$^aR(F) = \sum||F_o| - |F_c||/\sum|F_o|$. $^bR_w(F_o^2) = [\sum[w(F_o^2 - F_c^2)^2]/\sum wF_o^4]^{1/2}$.

dx.doi.org/10.1021/ja311910h | J. Am. Chem. Soc. 2013, 135, 2769−2775

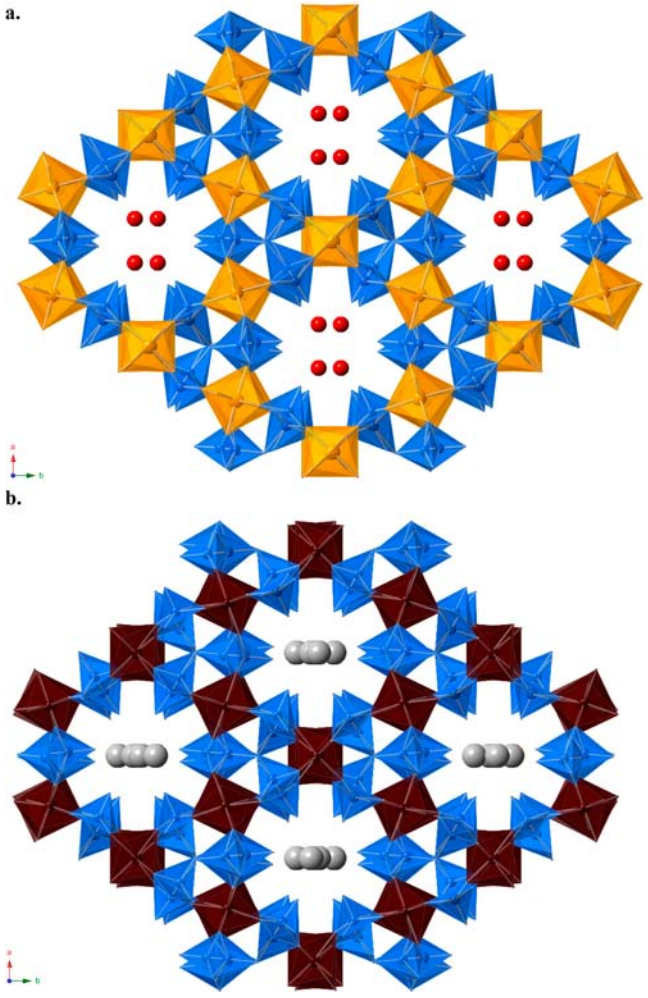

Figure 1. View down the *c* axis of $Ce_3Mo_6O_{24}(H_2O)_4$ (a) and $CsPu_3Mo_6O_{24}(H_2O)$ (b). Ce(IV) polyhedra are orange, Pu(IV) polyhedra are dark red, molybdate polyhedra are blue, oxygen atoms are red spheres, and Cs atoms are gray spheres.

The program CELL_NOW was used to detwin the data. Multiscan absorption corrections were applied using the program TWINABS.[55]

UV−vis−near-IR Spectroscopy. UV−vis−near-IR data were acquired from single or twinned crystals using a Craic Technologies microspectrophotometer. Crystals were placed on quartz slides under Krytox oil, and the data were collected from 200 to 1200 nm for $CsPu_3Mo_6O_{24}(H_2O)$ and from 200 to 950 nm for $Ce_3Mo_6O_{24}(H_2O)_4$.

SEM-EDS Analysis. Scanning electron microscopy/energy-dispersive spectroscopy (SEM/EDS) images and data were collected using a LEO Model EVO 50 system with an Oxford INCA energy-dispersive spectrometer. EDS indicated a 1:3:6 Cs:Pu:Mo ratio for the crystals of $CsPu_3Mo_6O_{24}(H_2O)$ and a 1:2 Ce:Mo ratio for $Ce_3Mo_6O_{24}(H_2O)_4$.

X-ray Absorption Studies. A crystalline sample of $CsPu_3Mo_6O_{24}(H_2O)$ was mounted in a triply nested slotted aluminum frame with sealed Kapton windows for the X-ray absorption studies. Spectra were measured at the Stanford Synchrotron Radiation Lightsource on beamline 11-2 using a half-tuned double Si(220) (ϕ = 0°) monochromator with 0.3 mm width vertical slits. Data were collected in fluorescence mode using a 30-element Ge detector, and all spectra were corrected for dead-time effects.

RESULTS AND DISCUSSION

Structure and Topological Description. $CsPu_3Mo_6O_{24}(H_2O)$ and $Ce_3Mo_6O_{24}(H_2O)_4$ both crystallize in the space group *C*2/*c* and share similar topologies. The main features of both structures are the channels that extend along the *c* axis. In $Ce_3Mo_6O_{24}(H_2O)_4$ these channels house water molecules, whereas in $CsPu_3Mo_6O_{24}(H_2O)$ the channels are smaller by approximately 1 Å across and contain disordered Cs^+ cations, as shown in Figure 1. The difference in channel size is reflected in the smaller volume of $CsPu_3Mo_6O_{24}(H_2O)$ at 2117(2) $Å^3$ versus $Ce_3Mo_6O_{24}(H_2O)$ at 2194.6(2) $Å^3$. The two structures each contain two unique RE atoms which are coordinated by eight O atoms, forming square antiprisms with approximate D_{4d} symmetry.[12,56] All O atoms in the $(RE)O_8$ polyhedra are donated from molybdate units. The $(RE)O_8$ polyhedra edge-share to form chains continuing down the *c* axis. The edge sharing alternates between aligning with the [*ac*] and [*bc*] planes between each polyhedron, as shown for both $CsPu_3Mo_6O_{24}(H_2O)$ and $Ce_3Mo_6O_{24}(H_2O)_4$ in Figure 2. The

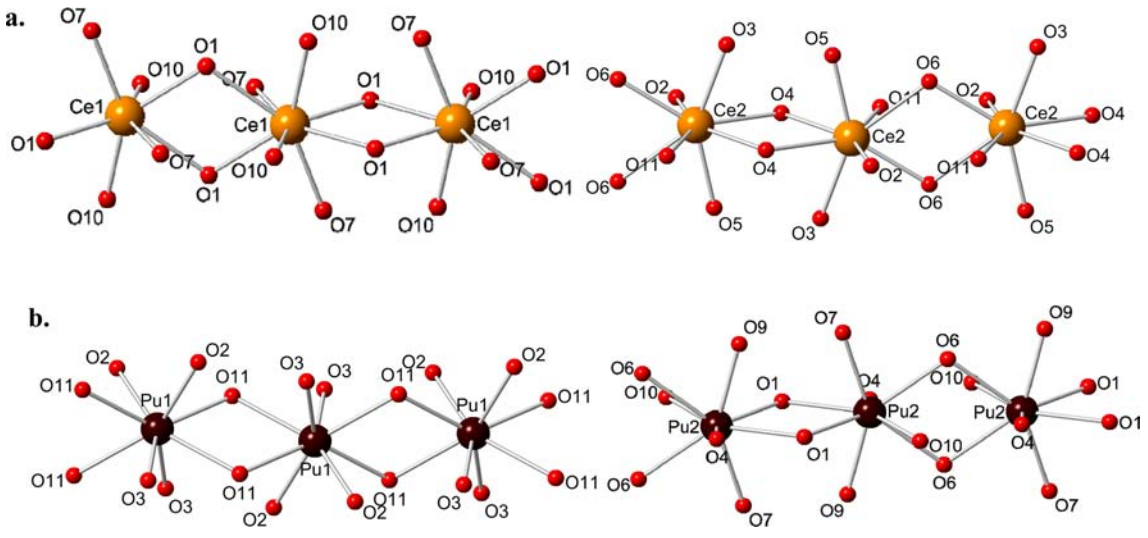

Figure 2. Coordination environments of the Ce(IV) (orange spheres) and Pu(IV) (dark red spheres) metal centers consisting of alternating edgee-sharing chains. All coordination environments are eight-coordinate square antiprisms with approximate D_{4d} symmetry. The chains are linked by molybdate polyhedra to build the framework.

dx.doi.org/10.1021/ja311910h | *J. Am. Chem. Soc.* 2013, 135, 2769−2775

Table 2. Selected Bond Distances (Å) for PuMoO and CeMoO

$Ce_3Mo_6O_{24}(H_2O)_4$		$CsPu_3Mo_6O_{24}(H_2O)$	
Ce(1)−O(10)	2.229(6)	Pu(1)−O(3)	2.257(11)
Ce(1)−O(10)	2.229(6)	Pu(1)−O(3)	2.257(11)
Ce(1)−O(1)	2.283(6)	Pu(1)−O(2)	2.315(9)
Ce(1)−O(1)	2.283(6)	Pu(1)−O(2)	2.315(9)
Ce(1)−O(7)	2.325(6)	Pu(1)−O(11)	2.320(9)
Ce(1)−O(7)	2.325(6)	Pu(1)−O(11)	2.320(9)
Ce(1)−O(1)	2.514(6)	Pu(1)−O(11)	2.410(8)
Ce(1)−O(1)	2.514(6)	Pu(1)−O(11)	2.410(8)
Ce(2)−O(5)	2.231(6)	Pu(2)−O(4)	2.234(11)
Ce(2)−O(11)	2.242(7)	Pu(2)−O(9)	2.257(10)
Ce(2)−O(2)	2.283(6)	Pu(2)−O(1)	2.313(8)
Ce(2)−O(6)	2.295(6)	Pu(2)−O(7)	2.322(9)
Ce(2)−O(3)	2.339(6)	Pu(2)−O(10)	2.369(9)
Ce(2)−O(4)	2.406(6)	Pu(2)−O(6)	2.372(8)
Ce(2)−O(4)	2.425(6)	Pu(2)−O(1)	2.427(8)
Ce(2)−O(6)	2.482(6)	Pu(2)−O(6)	2.433(8)
Mo(1)−O(9)	1.689(7)	Mo(1)−O(5)	1.660(12)
Mo(1)−O(7)	1.774(6)	Mo(1)−O(2)	1.758(9)
Mo(1)−O(6)	1.860(6)	Mo(1)−O(1)	1.860(8)
Mo(1)−O(10)	1.955(6)	Mo(1)−O(3)	1.940(10)
Mo(1)−O(5)	2.096(6)	Mo(1)−O(4)	2.090(10)
Mo(2A)−O(8)	1.608(7)	Mo(2A)−O(8)	1.667(14)
Mo(2A)−O(2)	1.791(6)	Mo(2A)−O(7)	1.741(8)
Mo(2A)−O(4)	1.877(6)	Mo(2A)−O(6)	1.882(9)
Mo(2A)−O(11)	2.027(7)	Mo(2A)−O(9)	2.013(11)
Mo(2A)−O(11)	2.061(6)	Mo(2A)−O(9)	2.089(10)
Mo(2B)−O(2)	1.717(6)	Mo(3A)−O(12)	1.686(13)
Mo(2B)−O(13B)	1.74(2)	Mo(3A)−O(10)	1.738(9)
Mo(2B)−O(4)	1.846(6)	Mo(3A)−O(11)	1.884(9)
Mo(2B)−O(11)	1.973(7)	Mo(3A)−O(4)	1.928(11)
Mo(2B)−O(11)	2.143(7)	Mo(3A)−O(3)	2.112(9)
Mo(2B)−O(13A)	2.360(14)	Mo(2B)−O(6)	1.856(9)
Mo(3A)−O(13A)	1.711(12)	Mo(2B)−O(7)	1.873(10)
Mo(3A)−O(3)	1.783(6)	Mo(2B)−O(9)	2.056(11)
Mo(3A)−O(1)	1.831(6)	Mo(2B)−O(9)	2.234(12)
Mo(3A)−O(5)	1.938(6)	Mo(3B)−O(10)	1.738(12)
Mo(3A)−O(10)	2.134(6)	Mo(3B)−O(11)	1.757(11)
Mo(3A)−O(13B)	2.22(2)	Mo(3B)−O(13B)	1.83(2)
Mo(3A)−O(12)	2.504(7)	Mo(3B)−O(4)	2.091(14)
Mo(3B)−O(12)	1.503(8)	Mo(3B)−O(13A)	2.203(16)
Mo(3B)−O(3)	1.791(6)	Mo(3B)−O(3)	2.334(12)
Mo(3B)−O(1)	1.901(6)	Mo(3B)−O(13A)	2.361(15)

average bond distances for the $Pu(1)O_8$ and $Pu(2)O_8$ polyhedra are 2.326(9) and 2.341(9) Å, respectively (Table 2). The average bond distances for the $Ce(1)O_8$ and $Ce(2)O_8$ polyhedra are both 2.338(6) Å. The molybdate oxoanions for both structures consist of MoO_5 square pyramids with the Mo(2) and Mo(3) sites disordered over two positions through a 180° rotation. These disordered sites are approximately 75%/25% occupied for Mo(2A)/Mo(2B) and approximately 85%/15% occupied for Mo(3A)/Mo(3B) sites in both studied structures. The Mo−O distances in $Mo(1)O_5$ groups present two short (1.66(1)−1.77(1) Å), one intermediate (1.86(7) Å), and two normal (1.94(1)−2.09(1) Å) bonds. $Mo(2A)O_5$ is quite similar to $Mo(1)O_5$ and has two short (1.61(1)−1.79(1) Å), one intermediate (1.882(9) Å), and two normal (2.01(1)−2.09(1) Å) Mo−O bonds. $Mo(3A)O_5$ groups are based on two short (1.68(1)−1.78(1) Å), one intermediate (1.831(6)−1.884(9) Å), one normal (1.93(1)−1.94(1) Å), and one long (2.112(9)−2.134(6) Å) Mo−O distances. The Mo(B) sites have been left out of the analysis for clarity. In $Ce_3Mo_6O_{24}(H_2O)_4$ Mo(1) edge-shares with Mo(3) to form a dimer and Mo(2) edge-shares with itself to also form a dimer. It would appear that Mo(3A) corner-shares with Mo(2B) through O(13), but O(13) is disordered over two sites as well. This could indicate that they are not oriented toward each other at the same time. Bond valence sums (BVS) are calculations using measured bond distances and predetermined bond valence parameters to determine the valence state of atoms in solid-state chemistry. BVS for Ce indicates a tetravalent oxidation state and BVS for all Mo sites indicate a hexavalent oxidation state (S1).[57] In $CsPu_3Mo_6O_{24}(H_2O)$ there are a similar topologies for Mo(1), Mo(2A), and Mo(3A) to $Ce_3Mo_6O_{24}(H_2O)_4$; however, the Mo(B) sites are different. To begin, the Mo−Mo disordered distances are larger by approximately 0.4 Å for Mo(2) and 0.09 Å for Mo(3). Additionally, Mo(3B), instead of Mo(3A), appears to corner-share with Mo(2B); this interaction is again through the disordered O(13), but the O(13) disorder distance is twice as long as it was in $Ce_3Mo_6O_{24}(H_2O)_4$, leading O(13B) to be disordered over a symmetry position. A comparison of molybdate coordination is shown in Figure 3. The BVS calculation for Pu in $CsPu_3Mo_6O_{24}(H_2O)$ indicates tetravalent Pu, while Mo BVS indicates hexavalent for all Mo sites except Mo(3B), which indicates Mo(V); however, the disordered O atoms make confident BVS assignments difficult. We have chosen to write the formula as it is shown with one Mo being pentavalent while the rest are hexavalent while making the disordered O13 a water molecule, since it has surplus electron density. BVS could not be used to locate any H atoms on O(13) because of the disorder. Writing the formula this way also highlights the placement of Cs in the channels instead of water, as it is needed to charge balance the pentavalent Mo. Addition of H atoms to compensate for disordered molybdate anions has been previously reported.[58−60]

UV−vis−near-IR Absorption Spectroscopy. The absorption spectrum for $CsPu_3Mo_6O_{24}(H_2O)$ was obtained from a very thin twinned crystal and is shown in Figure 4. The optical energy spectrum for $CsPu_3Mo_6O_{24}(H_2O)$ was obtained from a larger twinned crystal and is shown in Figure 5. The electronic transitions of f elements are well-known and have been characterized in the literature; however, the usual analysis fails here because of the dark color and very strong absorbance across the visible spectrum. However, the characteristic bands for Pu(IV) centered around 650 and 700 nm can be seen. Typical spectra of Pu(III) and Pu(IV) are found in the Supporting Information (S2). Using the absorbance data, absorbance vs optical energy plots were constructed to analyze the semiconductor nature of $CsPu_3Mo_6O_{24}(H_2O)$, as shown in Figure 5. The absorption energy curve was used to estimate the band gap at approximately 1.20 ± 0.03 eV by constructing a linear plot along the steep drop in absorbance highlighted in pink in Figure 5. The x intercept was then calculated from the equation of the constructed line. The absorption data of $Ce_3Mo_6O_{24}(H_2O)_4$ were similarly converted to optical energy, and the absorbance data can be found in the Supporting Information (S3 and S4). The band gap of $CsPu_3Mo_6O_{24}(H_2O)$ is smaller than the 1.8 eV band gap of PuO_2 but larger than the 0.55 eV band gap of Pu_2O_2X (X = S, Se).[61,62] The band gap for $Ce_3Mo_6O_{24}(H_2O)_4$ is much larger than that of $CsPu_3Mo_6O_{24}(H_2O)$ at 2.68 ± 0.02 eV.

XANES. Pu L3-edge XANES data for both the $CsPu_3Mo_6O_{24}(H_2O)$ crystal and the PuO_2 standard are shown in Figure 6. The

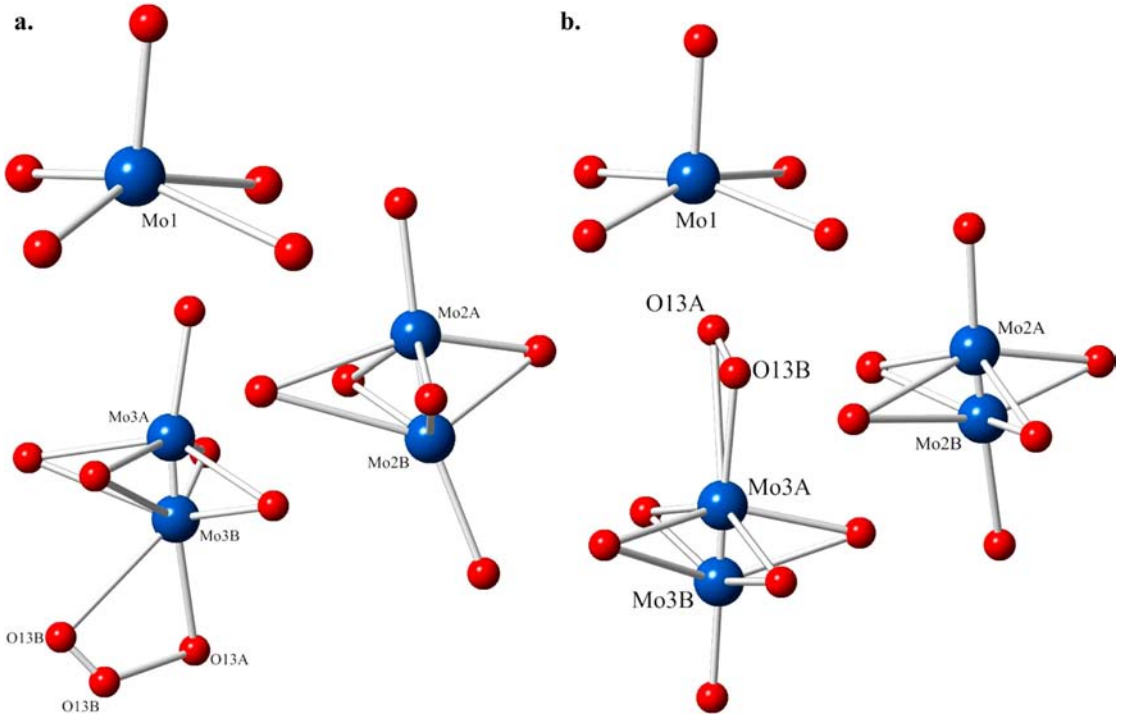

Figure 3. Coordination environments of Mo in $CsPu_3Mo_6O_{24}(H_2O)$ (a) and the coordination environment of Mo in $Ce_3Mo_6O_{24}(H_2O)_4$ (b). The square pyramid of Mo1 is not disordered in either structure, but the other molybdate units are disordered over two sites with 25% occupancy for Mo(2B) and 25% occupancy for Mo(3B). The disordered O(13) is also shown. Blue spheres represent Mo atoms, and red spheres represent O atoms.

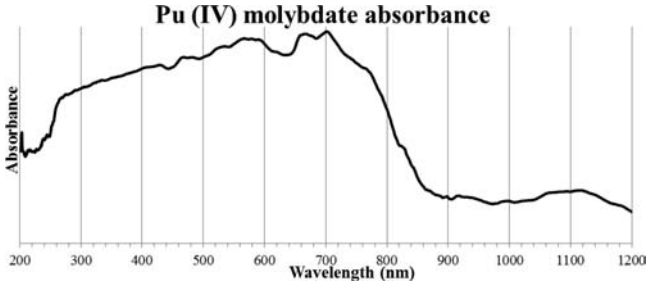

Figure 4. Absorption spectrum of $CsPu_3Mo_6O_{24}(H_2O)$ showing the strong absorbance from approximately 250 to 800 nm. The typical f−f transition analysis fails here, since those features are overwhelmed.

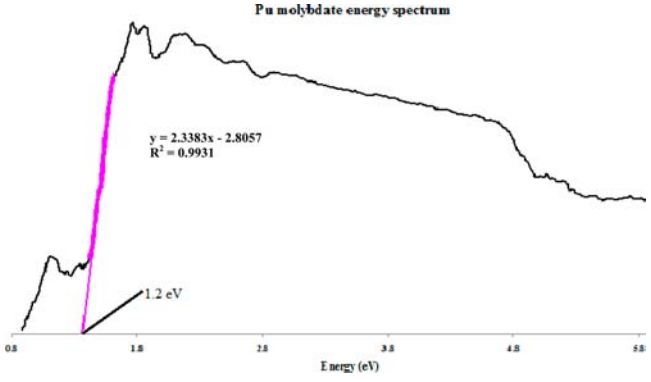

Figure 5. Optical energy spectrum of $CsPu_3Mo_6O_{24}(H_2O)$ used to determine the approximate band gap. The least-squares fit of the highlighted region is shown along with the *x* intercept that is the calculated band gap.

spectra are energy calibrated by setting the energy of the first inflection point of the PuO_2 standard to 18062.3 eV.[63] The strong

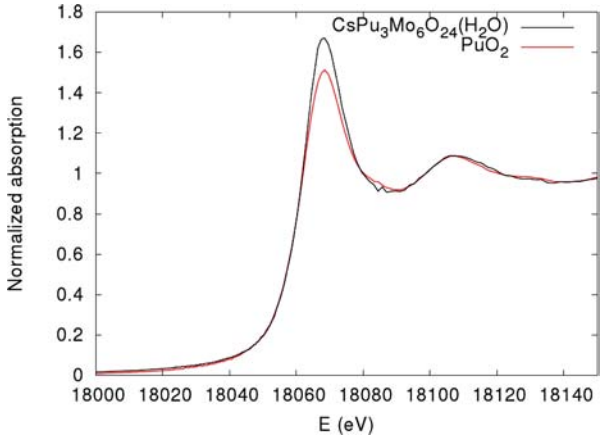

Figure 6. Pu XANES comparing the standard $Pu^{IV}O_2$ to $CsPu_3Mo_6O_{24}(H_2O)$, indicating that Pu is in the tetravalent state.

similarity between the data from the $CsPu_3Mo_6O_{24}(H_2O)$ crystal and PuO_2 indicates that the Pu in the $CsPu_3Mo_6O_{24}(H_2O)$ crystal is predominantly tetravalent Pu(IV). The typical shift in the white line position between Pu(III) and Pu(IV) systems is about 4 eV.[63] Note that the difference in the peak height of the main "white line" feature between the samples is commonly assigned to differences in the long-range electronic structure due to periodicity and is not indicative of a difference in valence.

The Mo K-edge XANES are shown in Figure 7 for the same crystal and a Mo foil standard. The energy is calibrated by setting the first inflection point from the Mo foil data to 20000.36 eV.[64] A large pre-edge feature labeled A is observed at 20006.6 eV, and the half-height is at about 20015.eV. There is also a feature labeled B at 20027(1) eV, and the white line is at about 20042(1) eV (broad and flat compared to A). Although

dx.doi.org/10.1021/ja311910h | J. Am. Chem. Soc. 2013, 135, 2769−2775

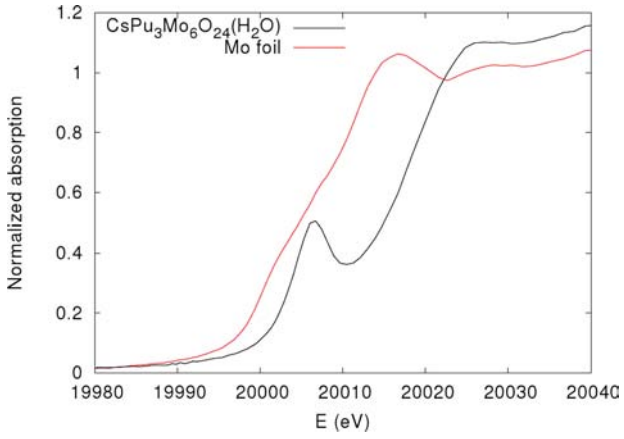

Figure 7. Mo K-edge XANES exhibiting a substantial pre-edge absorption peak, making analysis difficult. However, the energy at half-height of the edge indicates a Mo(V) or Mo(VI) valence.

the peak positions should be robust, the estimated half-height position from these XANES data is potentially affected by self-absorption. However, these samples are thin enough (the change in absorption at the Mo K edge corresponds to much less than one absorption length) that we estimate such a shift to be <0.1 eV.

The literature shows that while the Mo K edge is a typically good diagnostic for valence determination when the local geometry is relatively ordered, the large octahedral distortions that can occur around Mo can create very substantial pre-edge features (as observed here) that are far enough up on the main edge that the edge position as given by the position at the first inflection point is no longer very reliable for determining valence differences between Mo(V) and Mo(VI).[65−72,73] However, the energy at the half-height of the edge is better and indicates something close to Mo(VI), since Mo(IV) half-height energies are typically below 20011 eV when using our chosen energy calibration.[63,64] With such uncertainty, it is difficult to definitively interrogate the effective nuclear charge on the Mo ions; we therefore report here that the Mo K-edge XANES are consistent with a Mo(V,VI) state.

CONCLUSIONS

The two new f-block molybdates $Ce_3Mo_6O_{24}(H_2O)_4$ and $CsPu_3Mo_6O_{24}(H_2O)$ have been prepared hydrothermally and characterized. Although the two compounds have similar structural topologies, there are significant differences between the two compounds. $CsPu_3Mo_6O_{24}(H_2O)$ crystallizes as dark black-red plates that are semiconducting in nature, whereas $Ce_3Mo_6O_{24}(H_2O)_4$ crystallizes as bright yellow tablets with the typical wide gaps of insulating rare earth oxoanion compounds. Large channels are found in both compounds that house H_2O molecules in $Ce_3Mo_6O_{24}(H_2O)_4$ or Cs^+ cations in $CsPu_3Mo_6O_{24}(H_2O)$. X-ray absorption studies were undertaken to determine if mixed oxidation states were the reason for the black color of $CsPu_3Mo_6O_{24}(H_2O)$. XANES clearly indicates a tetravalent state for Pu; however, the distortion away from an octahedral geometry in Mo leads to large pre-edge absorption that prevented a definitive interrogation of the effective nuclear charge of the Mo ions. However, mixed-valent molybdenum is the most likely explanation for the dark color and explains the necessity of filling the channels with Cs^+ cations for charge compensation. This work represents a rather dramatic case where Ce(IV) does not properly model the behavior of Pu(IV). This particular example is quite different from others because previous deviations are observed in the local coordination environments of the f-block cations which include changes in coordination number, types of ligands, and site symmetry. Rather here, a different redox pathway yields mixed valency in the anionic network while the local environments of the Ce(IV) and Pu(IV) are virtually indistinguishable.

ASSOCIATED CONTENT

Supporting Information

CIF files, tables, and figures giving crystallographic information and calculated BVS values. This material is available free of charge via the Internet at http://pubs.acs.org.

AUTHOR INFORMATION

Corresponding Author

E-mail: talbrechtschmitt@gmail.com.

Notes

The authors declare no competing financial interest.

ACKNOWLEDGMENTS

We are grateful for support provided by the Materials Science of Actinides, an Energy Frontier Research Center funded by the U.S. Department of Energy (DOE), Office of Science (OS), Office of Basic Energy Sciences (OBES), under Award Number DE-SC0001089. Work at Lawrence Berkeley National Laboratory was supported by the Director, OS, OBES, of the DOE under Contract No. DE-AC02-05CH11231. X-ray absorption data were collected at the Stanford Synchrotron Radiation Lightsource, a national user facility operated by Stanford University on behalf of the DOE, OBES. Work at the Institute for Climate Research (IEK-6) and Energy was funded by Helmholtz Association Grant VH-NG-815.

REFERENCES

(1) Polinski, M. J.; Wang, S.; Alekseev, E. V.; Depmeier, W.; Albrecht-Schmitt, T. E. *Angew. Chem., Int. Ed.* **2011**, *50*, 8891−8894.
(2) Polinski, M. J.; Grant, D. J.; Wang, S.; Alekseev, E. V.; Cross, J. N.; Villa, E. M.; Depmeier, W.; Gagliardi, L.; Albrecht-Schmitt, T. E. *J. Am. Chem. Soc.* **2012**, *134*, 10682−10692.
(3) Polinski, M. J.; Wang, S.; Cross, J. N.; Alekseev, E. V.; Depmeier, W.; Albrecht-Schmitt, T. E. *Inorg. Chem.* **2012**, *51*, 7859−7866.
(4) Nelson, A.-G. D.; Bray, T. H.; Zhan, W.; Haire, R. G.; Sayler, T. S.; Albrecht-Schmitt, T. E. *Inorg. Chem.* **2008**, *47*, 4945−4951.
(5) Diwu, J.; Nelson, A.-G. D.; Albrecht-Schmitt, T. E. *Comments Inorg. Chem.* **2010**, *31* (112), 46−62.
(6) Diwu, J.; Nelson, A.-G. D.; Wang, S.; Albrecht-Schmitt, T. E. *Inorg. Chem.* **2010**, *49*, 3337−3342.
(7) Diwu, J.; Wang, S.; Liao, Z.; Burns, P. C.; Albrecht-Schmitt, T. E. *Inorg. Chem.* **2010**, *49*, 10074−10080.
(8) Diwu, J.; Wang, S.; Good, J.; Di Stefano, V. H.; Albrecht-Schmitt, T. E. *Inorg. Chem.* **2011**, *50*, 4842−4850.
(9) Diwu, J.; Good, J.; Di Stefano, V. H.; Albrecht-Schmitt, T. E. *Eur. J. Inorg. Chem.* **2011**, *9*, 1374−1377.
(10) Diwu, J.; Wang, S.; Albrecht-Schmitt, T. E. *Inorg. Chem.* **2012**, *51*, 4088−4093.
(11) Gorden, A. E. V.; Shuh, D. K.; Tiedemann, B. E. F.; Wilson, R. E.; Xu, J.; Raymond, K. N. *Chemistry* **2005**, *11*, 2842−2848.
(12) Gorden, A. E. V.; Xu, J.; Raymond, K. N. *Chem. Rev.* **2003**, *103*, 4207−4282.
(13) Xu, J.; Radkov, E.; Ziegler, M.; Raymond, K. N. *Inorg. Chem.* **2000**, *39*, 4156−4164.

(14) Szigethy, G.; Xu, J.; Gorden, A. E. V.; Teat, S. J.; Shuh, D. K.; Raymond, K. N. *Eur. J. Inorg. Chem.* **2008**, *13*, 2143−2147.
(15) Burns, J. H.; Peterson, J. R. *Acta Crystallogr.* **1970**, *B26*, 1885−1887.
(16) Burns, J. H.; Peterson, J. R.; Stevenson, J. N. *J. Inorg. Nucl. Chem.* **1975**, *37*, 743−749.
(17) Matonic, J. H.; Scott, B. L.; Neu, M. P. *Inorg. Chem.* **2001**, *40*, 2638−2639.
(18) Lindqvist-Reis, P.; Apostolidis, C.; Rebizant, J.; Morgenstern, A.; Klenze, R.; Walter, O.; Fanghaenel, T.; Haire, R. G. *Angew. Chem., Int. Ed.* **2007**, *46*, 919−922.
(19) Apostolidis, C.; Schimmelpfennig, B.; Magnani, N.; Lindqvist-Reis, P.; Walter, O.; Sykora, R.; Morgenstern, A.; Colineau, E.; Caciuffo, R.; Klenze, R.; Haire, R. G.; Rebizant, J.; Bruchertseifer, F.; Fanghanel, T. *Angew. Chem., Int. Ed.* **2010**, *49*, 343−6347.
(20) Peterson, J. R.; Burns, J. H. *J. Inorg. Nucl. Chem.* **1973**, *35*, 1525−1530.
(21) Milman, V.; Winkler, B.; Pickard, C. J. *J. Nucl. Mater.* **2003**, *322*, 165−179.
(22) Sykora, R. E.; Assefa, Z.; Haire, R. G.; Albrecht-Schmitt, T. E. *J. Solid State Chem.* **2004**, *177*, 4413−4419.
(23) Assefa, Z.; Haire, R. G.; Sykora, R. E. *J. Solid State Chem.* **2008**, *181*, 382−391.
(24) Skanthakumar, S.; Antonio, M. R.; Wilson, R. E.; Soderholm, L. *Inorg. Chem.* **2007**, *46*, 3485−3491.
(25) Cross, J. N.; Villa, E. M.; Wang, S.; Diwu, J.; Polinski, M. J.; Albrecht-Schmitt, T. E. *Inorg. Chem.* **2012**, *51*, 8419−8424.
(26) Opik, U.; Pryce, M. H. L. *Proc. R. Soc. London* **1937**, *A161*, 220.
(27) Wheeler, R. A.; Whangbo, M. H.; Hughbanks, T.; Hoffman, R.; Burdett, J. K.; Albright, T. A. *J. Am. Chem. Soc.* **1986**, *108*, 2222−2236.
(28) Pearson, R. G. *J. Mol. Struct.* **1983**, *103*, 25−30.
(29) Kang, S. K.; Tang, H.; Albright, T. A. *J. Am. Chem. Soc.* **1993**, *115*, 1971−1981.
(30) Cohen, R. E. *Nature* **1992**, *358*, 136−138.
(31) Burdett, J. K. *Molecular Shapes*; Wiley-Interscience: New York, 1980.
(32) Kunz, M.; Brown, I. D. J. *Solid State Chem.* **1995**, *115*, 395−406.
(33) Halasyamani, P. S.; Poeppelmeier, K. R. *Chem. Mater.* **1998**, *10*, 2753−2769.
(34) Penneman, R. A.; Haire, R. G.; Lloyd, M. H. In *Actinide Separations*; Navratil, J. D., Schulz, W. W., Eds.; American Chemical Society: Washington, DC, 1980; ACS Symposium Series *117*, pp 57−58.
(35) Buck, E. C.; Wronkiewicz, D. J.; Finn, P. A.; Bates, J. K. *J. Nucl. Mater.* **1997**, *249*, 70−76.
(36) Krivovichev, S. V.; Burns, P. C. *Structural Chemistry of Inorganic Actinides*; Elsevier: Amsterdam, 2007; Chapter 4, p 95.
(37) Pages, M.; Freundlich, W. *J. Inorg. Nucl. Chem.* **1972**, *34*, 2797−2801.
(38) Tabuteau, A.; Pages, M.; Freundlich, W. *Mater. Res. Bull.* **1972**, *7*, 691−697.
(39) Tabuteau, A.; Pages, M. *J. Solid State Chem.* **1978**, *26*, 153−158.
(40) Tabuteau, A.; Thevenin, T.; Pages, M. *Rev. Chim. Miner.* **1982**, *19*, 173−176.
(41) Dahale, N. D.; Keskar, M.; Mudher, S. K. D. *J. Alloys Compd.* **2006**, *415*, 244−250.
(42) Evans, J. S. O. *J. Chem. Soc., Dalton Trans.* **1999**, 3317−3326.
(43) Jeitschko, W. *Acta Crystallogr., Sect. B* **1972**, *28*, 60−76.
(44) Abrahams, S. C.; Svensson, C.; Bernstein, J. L. *J. Chem. Phys.* **1980**, *72*, 4278−4286.
(45) Hartenbach, I.; Strobel, S.; Dorhout, P. K.; Schleid, T. *J. Solid State Chem.* **2008**, *181*, 2828−2836.
(46) Hartenbach, I.; Strobel, S.; Dorhout, P. K.; Nockermann, P.; Binnemans, K.; Schleid, T. *Inorg. Chem.* **2008**, *47*, 3728−3735.
(47) Hartenbach, I.; Strobel, S.; Schleid, T.; Kramer, K. W.; Dorhout, P. K. *Z. Anorg. Allg. Chem.* **2009**, *635*, 966−975.
(48) Schleid, T.; Hartenbach, I. *Z. Anorg. Allg. Chem.* **2009**, *635*, 1904−1909.
(49) Hartenbach, I.; Strobel, S.; Schleid, T.; Dorhout, P. K. *Z. Anorg. Allg. Chem.* **2010**, *636*, 1183−1189.
(50) Brixner, L. H.; Sleight, A. W.; Licis, M. S. *J. Solid State Chem.* **1972**, *5*, 186−190.
(51) Manthiram, A.; Gopalakrishnan, J. *J. Less-Common Met.* **1984**, *99*, 107−111.
(52) Antonio, M. R.; Xue, J. S.; Soderholm, L. *J. Alloys Compd.* **1994**, *207/208*, 444−448.
(53) Antonio, M. R.; Staub, U.; Xue, J. S.; Soderholm, L. *Chem. Mater.* **1996**, *8*, 2673−2680.
(54) Antonio, M. R.; Xue, J. S.; Soderholm, L. *Chem. Mater.* **1995**, *7*, 333−340.
(55) Sheldrick, G. M. *Acta Crystallogr., Sect. A* **2008**, *A64*, 112−122.
(56) Kepert, D. L. *Prog. Inorg. Chem.* **1978**, *24*, 179−182.
(57) Brese, B. N.; O'Keefe, M. 1991, *B47*, 192-197.
(58) Zhang, X.; Wang, D.; Dou, J.; Yan, S.; Yao, X.; Jiang, J. *Inorg. Chem.* **2006**, *45*, 10629−10635.
(59) Long, D.; Kogerler, P.; Parenty, A. D. C.; Fielden, J.; Cronin, L. *Angew. Chem., Int. Ed.* **2006**, *45* (29), 4798−4803.
(60) Zhang, S.-Y.; Mao, J.-G. *Inorg. Chem.* **2011**, *50*, 4934−4943.
(61) McNeily, C. E. *J. Nucl. Mater.* **1964**, *11*, 53−58.
(62) Costantini, J. M.; Damien, D.; Novion, C. H.; Blaise, A.; Cousson, A.; Abazli, H.; Pages, M. *J. Solid State Chem.* **1983**, *47*, 210−218.
(63) Conradson, S. D.; Abney, K. D.; Begg, B. D.; Brady, E. D.; Clark, D. L.; den Auwer, C.; Ding, M.; Dorhout, P. K.; Espinosa-Faller, F. J.; Gordon, P. L.; Haire, R. G.; Hess, N. J.; Hess, R. F.; Keogh, D. W.; Lander, G. H.; Lupinetti, A. J.; Morales, L. A.; Neu, M. P.; Palmer, P. D.; Paviet-Hartmann, P.; Reilly, S. D.; Runde, W. H.; Tait, C. D.; Veirs, D. K.; Wastin, F. *Inorg. Chem.* **2004**, *43*, 116−131.
(64) Kraft, S.; Stumpel, J.; Becker, P.; Kuetgens, U. *Rev. Sci. Instrum.* **1996**, *67*, 681−688.
(65) George, G. N.; Kipke, C. A.; Prince, R. C.; Sunde, R. A.; Enemark, J. H.; Cramer, S. P. *Biochemistry* **1989**, *28*, 5075−5080.
(66) Jalilehvand, F.; Lim, B. S.; Holm, R. H.; Hedman, B.; Hodgson, K. O. *Inorg. Chem.* **2003**, *42*, 5531−5536.
(67) Jalilehvand, F.; Mah, V.; Leung, B. O.; Ross, D.; Parvez, M.; Aroca, R. F. *Inorg. Chem.* **2007**, *46*, 4430−4445.
(68) Kongmark, C.; Martis, V.; Pirovano, C.; Löfberg, A.; van Beek, W.; Sankar, G.; Rubbens, A.; Cristol, S.; Vannier, R.-N.; Bordes-Richard, E. *Catal. Today* **2010**, *157*, 257−262.
(69) Massa, M.; Häggbladd, R.; Hansen, S.; Andersson, A. *Appl. Catal. A: Gen.* **2011**, *408*, 63−72.
(70) Aritani, H.; Tanaka, T.; Funabiki, T.; Yoshida, S.; Kudo, M.; Hasegawa, S. *J. Phys. Chem.* **1996**, *100*, 5440−5446.
(71) Kutzler, F. W.; Scott, R. A.; Berg, J. M.; Hodgson, K. O.; Doniach, S.; Cramer, S. P.; Chang, C. H. *J. Am. Chem. Soc.* **1981**, *103*, 6083−6088.
(72) Antonio, M. R.; Teller, R. G.; Sandstrom, D. R.; Mehicic, M.; Brazdil, J. F. *J. Phys. Chem.* **1988**, *92*, 2939−2944.